

# Enhanced Electrochemical Water Oxidation: The Impact of Nano-clusters and Nano-cavities

Xueqing Zhang<sup>‡</sup>, Chonglong Cao,<sup>†\*</sup> Anja Bieberle-Hütter<sup>‡</sup>

<sup>†</sup> School of Physics and Technology, University of Jinan, Jinan, Shandong, 250022, People's Republic of China

<sup>‡</sup> Electrochemical Materials and Interfaces, Dutch Institute for Fundamental Energy Research (DIFFER), 5612AJ Eindhoven, the Netherlands

---

**Abstract:** The structures of transition metal surfaces and metal oxides are commonly believed to have significant effect on the catalytic reactions. Density functional theory calculations are therefore used in this study to investigate the oxygen evolution reaction (OER) over nanostructured, i.e. nano-cluster and nano-cavity, surfaces of hematite ( $\text{Fe}_2\text{O}_3$ ). The calculated results demonstrate an optimum nano-cluster size with respect to the OER overpotential. The presence of nano-clusters on the electrode is regarded as an attractive strategy for increasing the activity in photoelectrochemical water splitting. However, in this work, we found that the presence of nano-cavity is a more effective strategy into lowering the overpotential than nano-clusters. This finding of nano-cavity favoured OER for hematite surfaces is verified by similar simulations of  $\text{WO}_3$  surfaces.

**Keywords:** Oxygen evolution reaction, Density functional theory, Overpotential, Hematite, Tungsten oxide

---

## Introduction

Rational design of active oxygen evolution reaction (OER) catalysts is necessary for achieving sustainable energy conversion in systems, such as photoelectrochemical (PEC) fuel production.<sup>1-6</sup> Hematite ( $\alpha\text{-Fe}_2\text{O}_3$ ) has emerged as a promising photoelectrode material for PEC water splitting and received much attention due to its suitable band gap of about 2.1 eV, an excellent chemical stability in a broad pH range, its natural abundance, nontoxicity and low cost.<sup>2-4</sup> However, one main drawback of hematite as a photoelectrode material in PEC water splitting is its high overpotential for OER,<sup>4</sup> the reaction making the largest resistance to the electrolysis of water.<sup>7</sup> Many strategies have been proposed in the literature to increase the solar-to-hydrogen efficiency, such as controlling of the thin film thickness,<sup>8-10</sup> doping,<sup>11, 12</sup> nanostructures,<sup>13, 14 15, 16</sup> and altering the surface orientation.<sup>17, 18</sup> To further improve

the solar-to-hydrogen efficient, new strategies need to be found to make more efficient PEC interfaces.

Next to experimental studies, computational design at atomistic level can be achieved by the modern quantum chemical methods.<sup>19-22</sup> Computational strategies in designing of hematite photoelectrode have been reported by several groups. The effects of doping by Ti, Mn, Co, Ni, and Pt, on the overpotential have been investigated by Liao et al.<sup>23</sup> and Neufeld et al.<sup>24</sup> Co and Ni were predicted as effective dopants for electrocatalysis of water.<sup>23</sup> Nguyen et al.<sup>25</sup>, Hellman et al.<sup>26</sup> and Toroker et al.,<sup>27</sup> investigated water oxidation on hematite (0001) surface with vacancies. Nguyen et al.<sup>25</sup> and Hellman et al.<sup>26</sup> found that oxygen vacancies have significant effect on the overpotential. Nguyen et al.<sup>25</sup> found that Fe vacancies do not reduce the OER overpotential, whereas Toroker proposed that modulating iron vacancy concentration can serve as a means to control photoelectrochemical efficiency.<sup>27</sup> More recently, Zhang et al.<sup>28</sup> reported an overpotential of as low as 0.47 V for the hematite (110) surface with an oxygen vacancy concentration of 1.26 vacancies/nm<sup>2</sup>. Neufeld and Toroker studied the role of an  $\alpha$ -Al<sub>2</sub>O<sub>3</sub> and Ga<sub>2</sub>O<sub>3</sub> overlayer on Fe<sub>2</sub>O<sub>3</sub> for water splitting.<sup>29, 30</sup> An improvement of the electrochemical performance of the  $\alpha$ -Al<sub>2</sub>O<sub>3</sub> covered Fe<sub>2</sub>O<sub>3</sub> was found. The authors explained this improvement by the decrease in the work function of  $\alpha$ -Fe<sub>2</sub>O<sub>3</sub> upon  $\alpha$ -Al<sub>2</sub>O<sub>3</sub> coverage that aids in extracting electrons during the water oxidation reaction.<sup>29</sup>

Significant theoretical contributions have been made to simulate the OER at the hematite (0001) surface.<sup>18, 23-29, 31-40</sup> However, experimentally synthesised photoelectrodes are not in such pure surface condition.<sup>17</sup> Rather, they have many different orientations, nano-clusters/nano-cavities, grain boundaries, and defects.<sup>16, 41</sup> The nanostructures in general significantly affect their catalytic activity.<sup>42, 43</sup> Nanostructured surfaces were found experimentally to enhance the PEC activity significantly.<sup>1, 15, 16, 44</sup> On the theoretical side, Calle-Vallejo et al. found that concave geometries enhance the ORR activity over Pt (111) surface.<sup>45</sup> Similar theoretical investigations on the OER have not been reported so far. We focus, therefore, in this work on the theoretical understanding of the role of nano-cluster and -cavity on the OER using density functional theory calculations.

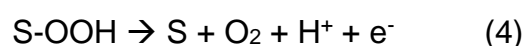
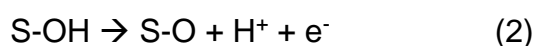
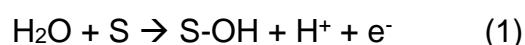
## Computational methods

Density functional theory (DFT) calculations have been performed using the ab-initio total-energy and molecular dynamics program VASP (Vienna Ab initio Simulation Package) developed by the Fakultät für Physik of the Universität Wien.<sup>46-50</sup> Since Fe<sub>2</sub>O<sub>3</sub> contains highly correlated 3d electrons, we chose the spin polarized DFT+U formalism<sup>23</sup> due to improper treatment of the d-electrons with standard DFT. The U value of 4.3 eV for Fe was derived in the literature<sup>23</sup> and has been applied to many hematite systems already.<sup>21, 24</sup> The Perdew–Burke–Ernzerhof (PBE) XC functional<sup>51</sup> and the projected augmented wave (PAW)<sup>47, 52</sup> potentials were used. A solid-gas model was used in this study similarly as in other OER studies of hematite.<sup>23-25</sup> More computational details are provided in the supporting information.

Several mechanisms are suggested for the OER on metal oxide surfaces in the literature.<sup>20</sup> Here we use the OER mechanism proposed by Rossmeisl et al.<sup>19</sup> This mechanism consists of four proton-coupled electron transfer (PCET) steps as shown in eq. (1-4). It has become very popular and has been shown to predict trends for the OER.<sup>20, 24, 53-56</sup>

At standard condition (U = 0, pH = 0, p = 1 bar, T = 298 K),  $\Delta G$  is  $\Delta G_0$  (the DFT calculated free energy). At a different condition,  $\Delta G = \Delta G_0 + \Delta G_U + \Delta G_{pH}$ . The effect of a bias on all states involving an electron in the electrode is included by shifting the energy of this state by  $\Delta G_U = -eU$ , where U is the electrode potential relative to the standard hydrogen electrode.<sup>19</sup>  $\Delta G_{pH} = -kT \cdot \ln[H^+] = kT \cdot 10 \cdot pH$ .

The four PCET steps are,



where S is the active site at the electrode surface. The entire process has an energy change of 4.92 eV (i.e. 1.23 eV for each PCET step). More details regarding the calculation of the energies can be found in the supporting information.

According to the method described in ref.<sup>19</sup> the oxygen evolution reaction (OER) overpotential is determined by

$$\eta = \max[\Delta G_n]/e - 1.23 \text{ [V]} \quad (5)$$

where  $\Delta G$  signifies the free energy with the active site as the reference.  $n$  is the number of reactions considered in the system and  $\Delta G_n$  is the free energy step for a single reaction.

## Results and discussion

Figure 1 shows the molecular geometries of five nano-cluster systems investigated in this work with the example species, OH, adsorbed at the active site. Each system consisted of three layers of  $\text{Fe}_2\text{O}_3$  in (110) orientation with the same initial geometry. The top layers consisted of 1 Fe atom, 5 Fe atoms, 8 Fe atoms, 11 Fe atoms, and 15 Fe atoms, respectively. The geometries after optimization are shown in Figure 1 (a-e). The cluster shown in Figure 1 (e) was optimized firstly. Based on this geometry, the Fe and O atoms (in the ratio of 2/3) of the top layer were removed and the geometry was relaxed again to build the smaller clusters. The free energies of the four intermediate steps were calculated.

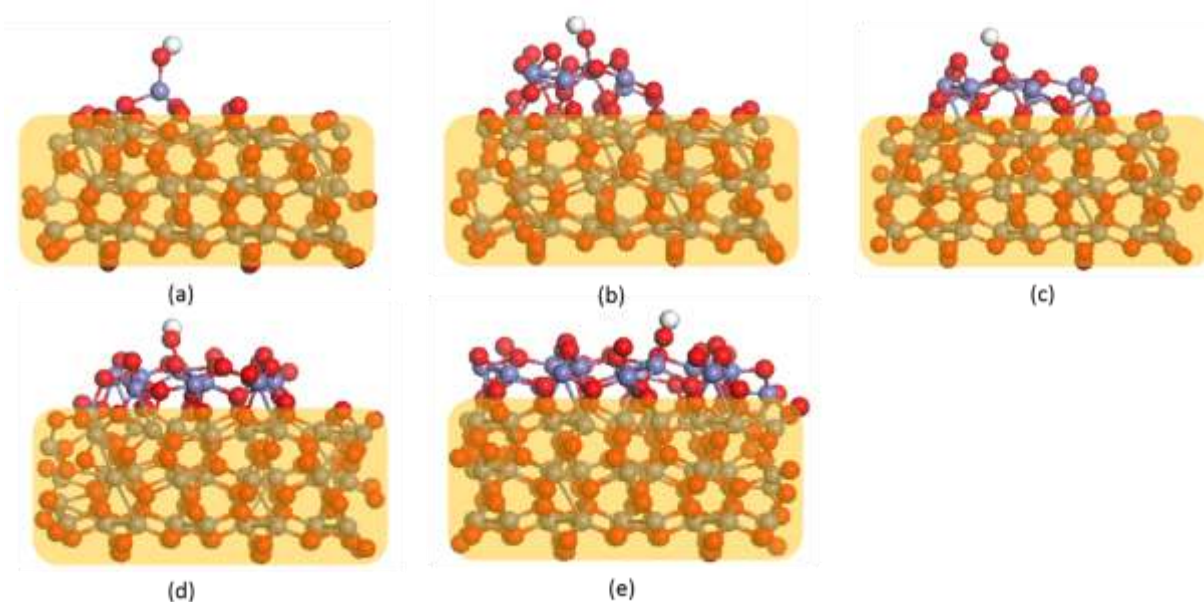


Figure 1. The five example geometries of  $\text{Fe}_2\text{O}_3$  nano-clusters with OH adsorbed. The nano-clusters consist of 3 layers  $\text{Fe}_2\text{O}_3$  (coloured in light yellow) and a top layer of different size. The size of the top layer is characterized by the number of Fe atoms. a) 1 Fe atom, b) 6 Fe atoms, c) 9 Fe atoms, d) 12 Fe atoms, and (e) 15 Fe atoms. Colour coding: red (O), blue (Fe) and white (H).

Figure 2 shows the free energy profiles of the four proton coupled electron transfer (PCET) steps using the approach developed by Rossmeisl and Norskov et

al.<sup>19</sup> From Figure 2, it is apparent that the size of the top layer has significant effect on the energies of the intermediate species and, hence, significantly influences the overpotential. The potential determining step of nano-cluster (b) is the OH formation, while the O formation is limiting for the rest of the nano-clusters. With the increase of the nano-cluster size from (a) to (c) the overpotential decreases from to 1.10 V to 0.77 V. The overpotential of nano-clusters (d) and (e) are both higher than that of (c). Thus, the best performance is found for nano-cluster (c) with a top layer of 8 Fe atoms. It is noteworthy that most of the nano-clusters studied are less active than the flat hematite (110) surface with an overpotential of 0.79 V.<sup>28</sup> The only exception is nano-cluster (c) which is a little more active than the flat surface; the overpotential of nano-cluster (c) is only 0.02 V lower than that of flat surface. Such a small difference is negligible considering the accuracy of DFT. To conclude, creating nano-clusters is not an efficient way to enhance the OER activity at hematite (110) surfaces. Although designing of nano-clusters increases the surface area and thus the number of active sites, the nano-clusters itself do not lower the OER overpotential efficiently.

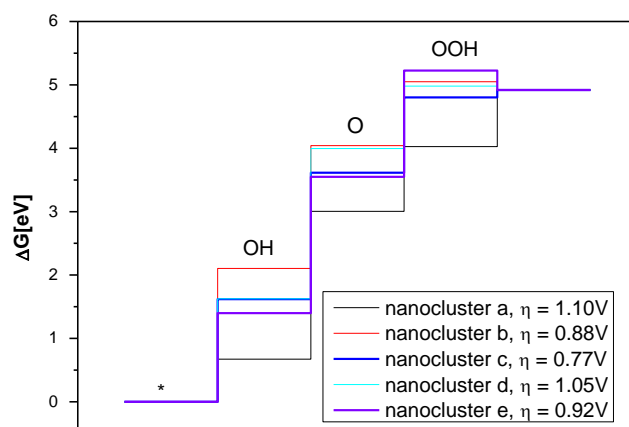


Figure 2. Calculated free energy profiles for OER intermediate species at five nano-clusters with different sizes as shown in Figure 1.

To further explore the impact of local geometries on the OER overpotential, we investigate the effect of nano-cavities. A nano-cavity is created by removing four  $\text{Fe}_2\text{O}_3$  units from the hematite (110) surface (Figure 3). The colour of the top layer is changed for guiding the eye. The depth is determined by removing one layer of O-Fe. The size of the cavity was chosen based on pre-calculation tests: several smaller cavities were

chosen. The calculations show that when the cavity is too small the adsorbed intermediate species form bonds with the step edges. The cavity cannot be too large. Otherwise the totally system will be too large and thus computationally too expensive.

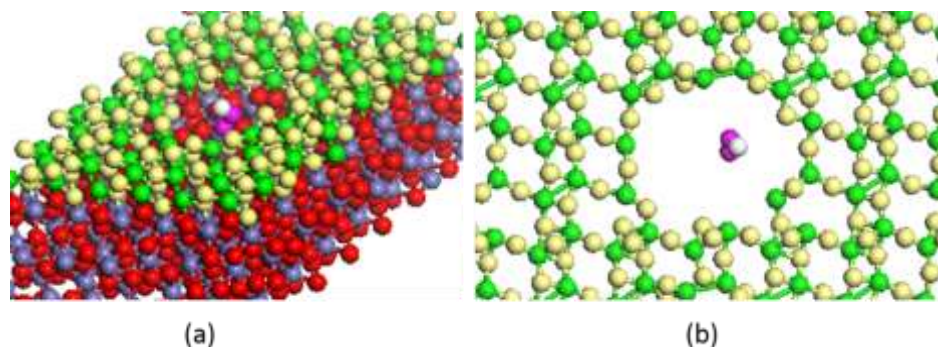


Figure 3. Hematite (110) surface with nano-cavity and adsorbed OOH in the middle of the cavity: (a) full structure with 120 Fe atoms (top-side view). The colour of the top layer is changed for guiding the eye, (b) top layer only (top view). Colour coding: red (O), blue (Fe) and white (H), green (Fe), yellow (O), and purple (O of the adsorbed OOH).

Figure 4 shows the comparison of free energy profile between nano-cavity and flat surface (data for the flat surface is from literature<sup>28</sup>). In general, the presence of the nano-cavity destabilizes the intermediate species, i.e. the free energy levels for each step are higher compared to the flat surface. The potential determining step is the formation of O for both cases (the largest step is from OH to O, eq. 2). At the cavity site, the OH is more destabilized than O. Thus, this destabilization makes the potential determining step smaller compared to the flat surface as shown in Figure 4. Hence, the overpotential is decreased by 0.16 V compared to the flat surface. This is a significant step in decreasing overpotential.

In summary, the designing of nano-cavities is more efficient in lowering the OER overpotential than nano-clusters. This trend is in good agreement with the findings for oxygen reduction reaction (ORR) over Pt (111) surface.<sup>45</sup> The authors found that the presence of a nano-cavity decreased the ORR overpotential by 0.15 V. Therefore, nano-cavities are recommended to enhance the ORR activity. The increase in activity was attributed to the difference in coordination numbers.<sup>45</sup> With our study, we can confirm this trend for OER on hematite surfaces. However, the geometry of hematite is too complicated to assign a Fe atom as the first (or second) neighbour of a selected Fe atom due to very diverse Fe-Fe distances as shown in Figure S1 of the Supporting Information. In order to verify this dependence for the OER activity we study this

dependence in one of the following subsection with the  $\text{WO}_3$  system which has a more well-defined geometry.

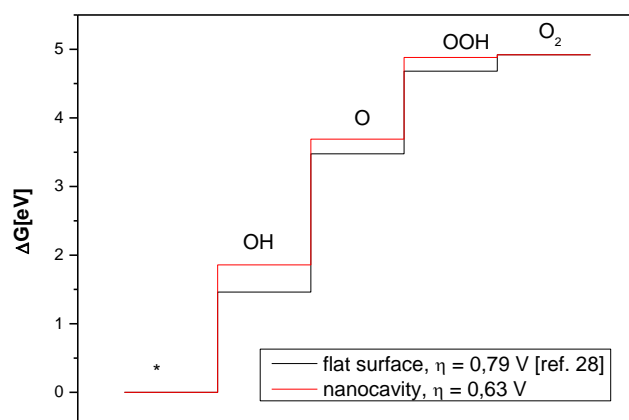


Figure 4. Calculated free energy profile for OER intermediate species at hematite (110) surface with the nanocavity as shown in Figure 3. The data of flat hematite (110) surface is included for comparison.<sup>28</sup>

Figure 5 summarizes all calculated overpotentials for the nanostructured hematite systems. As the size of the nano-cluster increases, the OER overpotential decreases from 1.10 to 0.77V and then increases and decrease again. Although there is no clear trend in the size dependence of overpotential, it is apparent that nano-clusters do not favour OER. The best candidate is nano-cluster (c) with an 8 Fe atom top layer. The overpotential is only 0.02 V lower than that of the flat surface. In contrast, the overpotential of a geometry with a nano-cavity is lower than all the nano-clusters considered in this study.

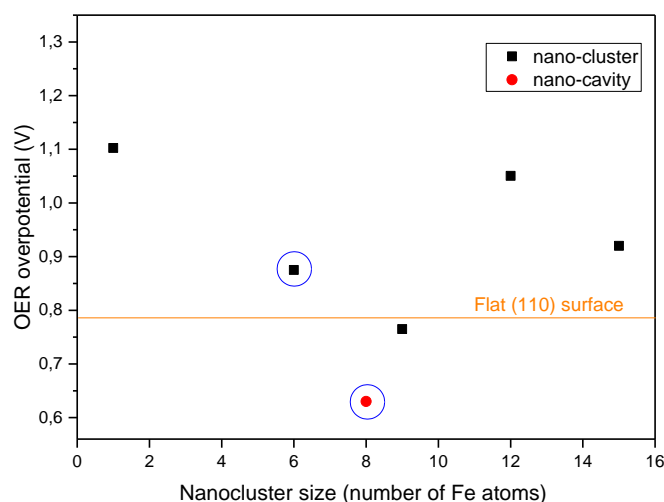


Figure 5. Calculated overpotential as a function of nanocluster/-cavity size. Nanoclusters are shown in black, the nano-cavity is shown in red. Usually O formation is limiting; the circles indicate that OH formation limiting.

To verify the conclusion of the nano-cavity favoured OER activity, we performed simulations of free energy steps of PCET for a  $\text{WO}_3$  (200) surface with a nano-cavity. Experimentally synthesised  $\text{WO}_3$  crystals are dominated by (200), (020), and (002) orientations.<sup>57, 58</sup> The (200) surface has been predicted the most active orientation theoretically.<sup>59</sup> The calculated overpotential for the flat (200) surface is 1.04 V.<sup>59</sup> Figure 6 shows an example geometry of the  $\text{WO}_3$  (200) surface with the OOH adsorbed on a cavity site. The calculated overpotential is 0.75 V, which is lower than that of the  $\text{WO}_3$  (200) flat surface. This means that the OER activity is, similarly as for the hematite surface, enhanced by the presence of a nano-cavity.

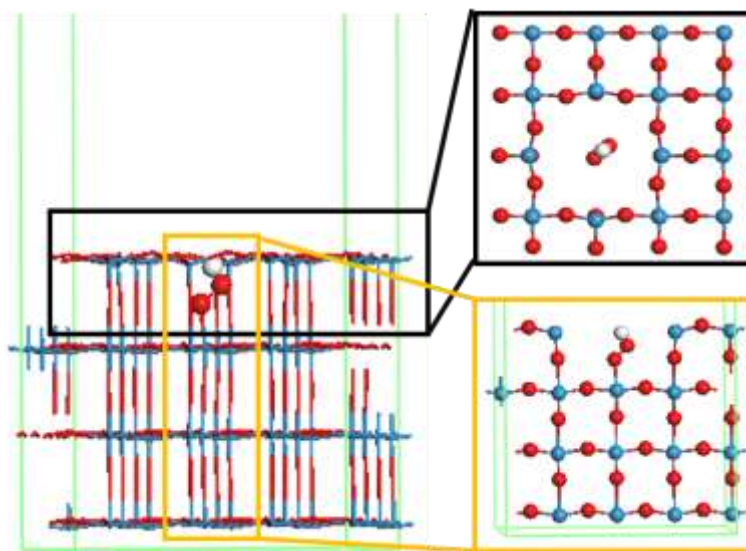


Figure 6. The geometries of the  $\text{WO}_3$  (200) surface with a nano-cavity. Left, the slab with the adsorbed OOH presented in balls; all other atoms are illustrated as lines. For a clear view of the cavity, the top layer (right above) and the cross section layer (right below) are shown.

Calle-Vallejo et al.<sup>45</sup> found that the sites with the same number of first-nearest neighbors as Pt (111) terraces, but with an increased number of second-nearest neighbors have superior catalytic activity for ORR. Here, we compare the first-nearest neighbors (W atoms) and second-nearest neighbors for the  $\text{WO}_3$  (200) surfaces with and without a nano-cavity having overpotentials of 1.04 V (ref. <sup>59</sup>) and 0.75 V (calculation in this study), respectively. Figure 7 shows the first and second nearest neighbors of  $\text{WO}_3$  (200) surfaces with and without nano-cavity. The active site is in each image highlighted with a green circle. Figure 7 (a) and (b) show the first-nearest W neighbors of the active site without cavity and with cavity, respectively. Both

geometries have five first-nearest neighbors. For the second-nearest neighbors, the situation is different: whereas the geometry without nano-cavity has eight second-nearest neighbors (Figure 7(c)), the geometry with nano-cavity has twelve second-nearest neighbors (Figure 7 (d)). Hence, the OER activity follows the same trend as observed by Calle-Vallejo et al.<sup>45</sup> for the ORR at Pt (111) terraces: The structure with cavity and increased second-nearest neighbors, namely 12, favour the electrochemical reactions and has a lower overpotential (0.75 V) compared to the structure without cavity and less second-nearest neighbors, namely 8 (1.04 V) <sup>59</sup>.

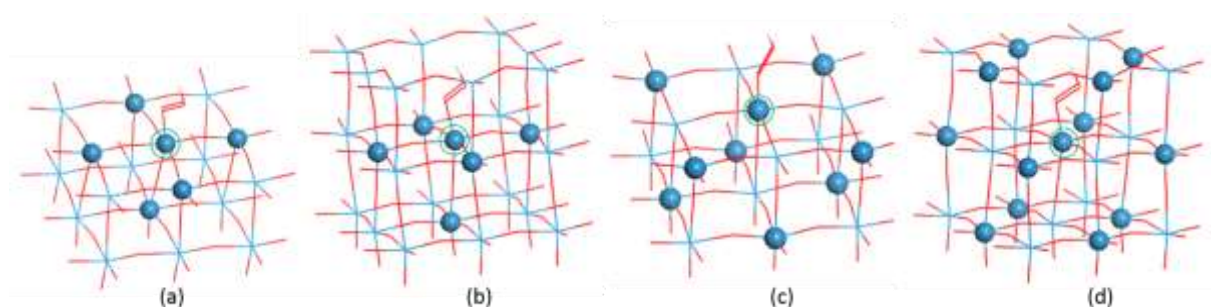


Figure 7. Comparison of the first-nearest neighbors and second-nearest neighbors for the WO<sub>3</sub> (200) surfaces with and without a nano-cavity. (a) first-nearest neighbors without cavity, (b) first-nearest neighbors with a cavity, (c) second-nearest neighbors without cavity, (d) second-nearest neighbors with a cavity. The green circle indicates the active site.

Improving OER efficiency through nanoscopic confinement has recently been discovered by Doyle and Vojvodic et al.<sup>60</sup> The authors proposed a scheme to study the effects of confinement by defining a channel in a three-dimensional nanoscopic catalyst structure. The channel was shown to lower overpotential for the OER, increasing catalytic efficiency. The effect of cavity on OER is in line with this nanoscopic confinement. The cavity can destabilize HO\* relative to O\*, and therefore decrease the potential determining step as shown in Figure 4.

## Summary

In summary, density functional theory calculations have been performed to search for new strategies towards lowering the OER overpotential in photoelectrochemical water splitting. Nanostructured hematite systems (nano-clusters and nano-cavities) have been investigated. The calculations show that the nano-cluster size influence OER overpotential, however, it does not reduce the overpotential significantly compared with the flat hematite surface. Hematite surfaces with a nano-cavity are, however, more

active than both flat surface and surfaces with nano-clusters. We demonstrate for the first time that the OER overpotential is reduced by 0.16 V at a cavity site with respect to the flat hematite surface. This conclusion for hematite was verified with another material by simulating the OER at a cavity site of WO<sub>3</sub> (200) surface. We found that also for the WO<sub>3</sub> surface, the nano-cavity decreased the overpotential. This increase in the OER activity was related to an increased number of second-nearest neighbors. The finding is also in line with the discovery of the effect of nanoscopic confinement on lowering the OER overpotential.

## ACKNOWLEDGMENTS

Zhang and Bieberle-Hütter acknowledge the financial support from NWO (FOM program nr. 147 “CO<sub>2</sub> neutral fuels”) for carrying out this study. Cao acknowledges the financial support from the Natural Science Foundation of Shandong Province (Grant No. ZR2015AL020). Supercomputing facilities of the Dutch national supercomputers SURFsara/Lisa and Cartesius are acknowledged.

## References

1. R. van de Krol, Y. Liang and J. Schoonman, *J. Mater. Chem.*, 2008, **18**, 2311-2320.
2. L. Jia, K. Harbauer, P. Bogdanoff, I. Herrmann-Geppert, A. Ramirez, R. van de Krol and S. Fiechter, *Journal of Materials Chemistry A*, 2014, **2**, 20196-20202.
3. F. Le Formal, E. Pastor, S. D. Tilley, C. A. Mesa, S. R. Pendlebury, M. Grätzel and J. R. Durrant, *J. Am. Chem. Soc.*, 2015, **137**, 6629-6637.
4. K. Sivula, F. Le Formal and M. Grätzel, *ChemSusChem*, 2011, **4**, 432-449.
5. Y. Jiao, Y. Zheng, M. Jaroniec and S. Z. Qiao, *Chem. Soc. Rev.*, 2015, **44**, 2060-2086.
6. Y. P. Zhu, Y. Jing, A. Vasileff, T. Heine and S.-Z. Qiao, *Advanced Energy Materials*, 2017, DOI: 10.1002/aenm.201602928, 1602928-n/a.
7. M. G. Walter, E. L. Warren, J. R. McKone, S. W. Boettcher, Q. Mi, E. A. Santori and N. S. Lewis, *Chem. Rev.*, 2010, **110**, 6446-6473.
8. F. Le Formal, M. Grätzel and K. Sivula, *Adv. Funct. Mater.*, 2010, **20**, 1099-1107.
9. O. Zandi, J. A. Beardslee and T. Hamann, *The Journal of Physical Chemistry C*, 2014, **118**, 16494-16503.
10. T. Hisatomi, H. Dotan, M. Stefiik, K. Sivula, A. Rothschild, M. Grätzel and N. Mathews, *Adv. Mater.*, 2012, **24**, 2699-2702.
11. X. Zhang, H. Li, S. Wang, F.-R. F. Fan and A. J. Bard, *The Journal of Physical Chemistry C*, 2014, **118**, 16842-16850.
12. K. D. Malviya, H. Dotan, D. Shlenkevich, A. Tsyganok, H. Mor and A. Rothschild, *Journal of Materials Chemistry A*, 2016, **4**, 3091-3099.
13. J. Brilliet, M. Grätzel and K. Sivula, *Nano Lett.*, 2010, **10**, 4155-4160.
14. T. K. Townsend, E. M. Sabio, N. D. Browning and F. E. Osterloh, *Energy & Environmental Science*, 2011, **4**, 4270-4275.
15. Y. Qiu, S.-F. Leung, Q. Zhang, B. Hua, Q. Lin, Z. Wei, K.-H. Tsui, Y. Zhang, S. Yang and Z. Fan, *Nano Lett.*, 2014, **14**, 2123-2129.
16. S. C. Warren, K. Voitchovsky, H. Dotan, C. M. Leroy, M. Cornuz, F. Stellacci, C. Hébert, A. Rothschild and M. Grätzel, *Nat Mater*, 2013, **12**, 842-849.
17. S. Kment, P. Schmuki, Z. Hubicka, L. Machala, R. Kirchgeorg, N. Liu, L. Wang, K. Lee, J. Olejnicek, M. Cada, I. Gregora and R. Zboril, *ACS Nano*, 2015, **9**, 7113-7123.

18. X. Zhang, C. Cao and A. Bieberle-Hütter, *The Journal of Physical Chemistry C*, 2016, **120**, 28694-28700.
19. J. Rossmeisl, Z. W. Qu, H. Zhu, G. J. Kroes and J. K. Nørskov, *J. Electroanal. Chem.*, 2007, **607**, 83-98.
20. X. Zhang and A. Bieberle-Hütter, *ChemSusChem*, 2016, **9**, 1223-1242.
21. P. Liao and E. A. Carter, *Chem. Soc. Rev.*, 2013, **42**, 2401-2422.
22. A. V. Akimov, A. J. Neukirch and O. V. Prezhdo, *Chem. Rev.*, 2013, **113**, 4496-4565.
23. P. Liao, J. A. Keith and E. A. Carter, *J. Am. Chem. Soc.*, 2012, **134**, 13296-13309.
24. O. Neufeld and M. C. Toroker, *The Journal of Physical Chemistry C*, 2015, **119**, 5836-5847.
25. M.-T. Nguyen, S. Piccinin, N. Seriani and R. Gebauer, *ACS Catalysis*, 2015, **5**, 715-721.
26. A. Hellman, B. Iandolo, B. Wickman, H. Grönbeck and J. Baltrusaitis, *Surf. Sci.*, 2015, **640**, 45-49.
27. M. C. Toroker, *The Journal of Physical Chemistry C*, 2014, **118**, 23162-23167.
28. X. Zhang, P. Klaver, R. van Santen, M. C. M. van de Sanden and A. Bieberle-Hütter, *The Journal of Physical Chemistry C*, 2016, **120**, 18201-18208.
29. O. Neufeld, N. Yatom and M. Caspary Toroker, *ACS Catalysis*, 2015, **5**, 7237-7243.
30. E. Aharon and M. C. Toroker, *Catal. Lett.*, 2017, **147**, 2077-2082.
31. P. Liao, M. C. Toroker and E. A. Carter, *Nano Lett.*, 2011, **11**, 1775-1781.
32. M.-T. Nguyen, N. Seriani, S. Piccinin and R. Gebauer, *The Journal of Chemical Physics*, 2014, **140**, 064703.
33. M.-T. Nguyen, M. Farnesi Camellone and R. Gebauer, *The Journal of Chemical Physics*, 2015, **143**, 034704.
34. O. Neufeld and M. C. Toroker, *PCCP*, 2015, **17**, 24129-24137.
35. M.-T. Nguyen, N. Seriani and R. Gebauer, *ChemPhysChem*, 2014, **15**, 3136-3136.
36. N. Yatom, O. Neufeld and M. Caspary Toroker, *The Journal of Physical Chemistry C*, 2015, **119**, 24789-24795.
37. K. Ulman, M.-T. Nguyen, N. Seriani and R. Gebauer, *The Journal of Chemical Physics*, 2016, **144**, 094701.
38. N. Yatom and M. Toroker, *Molecules*, 2015, **20**, 19668.
39. N. Yatom, Y. Elbaz, S. Navon and M. Caspary Toroker, *PCCP*, 2017, **19**, 17278-17286.
40. L. K. Jakobsson, G. Tranell and I.-H. Jung, *Metallurgical and Materials Transactions B*, 2017, **48**, 60-72.
41. A. Kay, I. Cesar and M. Grätzel, *J. Am. Chem. Soc.*, 2006, **128**, 15714-15721.
42. F. Zaera, *Chem. Soc. Rev.*, 2013, **42**, 2746-2762.
43. P. Christopher, H. Xin and S. Linic, *Nat Chem*, 2011, **3**, 467-472.
44. F. Jiao and H. Frei, *Energy & Environmental Science*, 2010, **3**, 1018-1027.
45. F. Calle-Vallejo, J. Tymoczko, V. Colic, Q. H. Vu, M. D. Pohl, K. Morgenstern, D. Loffreda, P. Sautet, W. Schuhmann and A. S. Bandarenka, *Science*, 2015, **350**, 185-189.
46. <https://www.vasp.at/>.
47. G. Kresse and D. Joubert, *Physical Review B*, 1999, **59**, 1758-1775.
48. O. Bengone, M. Alouani, P. Blöchl and J. Hugel, *Physical Review B*, 2000, **62**, 16392-16401.
49. G. Kresse and J. Furthmüller, *Comput. Mater. Sci.*, 1996, **6**, 15-50.
50. G. Kresse and J. Furthmüller, *Physical Review B*, 1996, **54**, 11169-11186.
51. J. P. Perdew, K. Burke and M. Ernzerhof, *Phys. Rev. Lett.*, 1996, **77**, 3865-3868.
52. P. E. Blöchl, *Physical Review B*, 1994, **50**, 17953-17979.
53. A. Valdes, J. Brillet, M. Gratzel, H. Gudmundsdottir, H. A. Hansen, H. Jonsson, P. Klupfel, G.-J. Kroes, F. Le Formal, I. C. Man, R. S. Martins, J. K. Nørskov, J. Rossmeisl, K. Sivula, A. Vojvodic and M. Zach, *PCCP*, 2012, **14**, 49-70.
54. R. Frydendal, M. Busch, N. B. Halck, E. A. Paoli, P. Krtil, I. Chorkendorff and J. Rossmeisl, *ChemCatChem*, 2015, **7**, 149-154.
55. F. Calle-Vallejo, O. A. Díaz-Morales, M. J. Kolb and M. T. M. Koper, *ACS Catalysis*, 2015, **5**, 869-873.
56. X. Zhou, E. J. M. Hensen, R. A. van Santen and C. Li, *Chemistry – A European Journal*, 2014, **20**, 6915-6926.
57. C. Santato, M. Odziemkowski, M. Ulmann and J. Augustynski, *J. Am. Chem. Soc.*, 2001, **123**, 10639-10649.
58. Q. Mi, Y. Ping, Y. Li, B. Cao, B. S. Brunschwig, P. G. Khalifah, G. A. Galli, H. B. Gray and N. S. Lewis, *J. Am. Chem. Soc.*, 2012, **134**, 18318-18324.
59. Á. Valdés and G.-J. Kroes, *The Journal of Chemical Physics*, 2009, **130**, 114701.
60. A. D. Doyle, J. H. Montoya and A. Vojvodic, *ChemCatChem*, 2015, **7**, 738-742.